Further Investigation of a Frequency-Reconfigurable Transponder on the Basis of a Mutually Coupled Antenna Cluster and Phased Modulators

T. A. Siddiqui, P. Khanal, J. Holopainen, and V. Viikari

Abstract – In this article, a frequency-reconfigurable transponder on the basis of the antenna cluster and phased modulators is presented. Frequency reconfigurability is obtained through a cluster of mutually coupled antenna elements of variable length. The approach benefits from mutual coupling instead of avoiding it. By optimally delaying the modulated reflected signal at each antenna element in the time domain (i.e., phase shift in the frequency domain) through the modulation delay, the backscattered signal power can be maximized at a given frequency. The broadband transponder is intended to function over a wide frequency range of 1 GHz to 6 GHz.

1. Introduction

Transponders incorporating an ambient backscatter communication principle use existing RF signals (TV towers, FM towers, cellular base stations, Bluetooth, and Wi-Fi access points) for operation without the deployment of dedicated RF transmitters [1–3]. Due to the dynamic nature of RF ambient signals in terms of location and transmit power, it is very challenging to achieve efficient operation over all the frequency bands, leading to the concept of a frequency-reconfigurable transponder that operates over a wide frequency range. The weighting techniques in [4] have been used to improve antenna efficiency in a coupled environment, but it is not directly applicable to the transponder case. Traditional transponders using a modulated backscattering principle operate at a narrowband due to fixed antennas, especially due to modulators, whose impedance cannot be modified. If broadband modulation is required, the power consumption of the modulator is greatly increased. A frequency-reconfigurable transponder on the basis of the antenna cluster, tuned into multiple bands in this case, exploits the ambient RF signals more efficiently. Different approaches to achieve the frequency reconfigurability include tunable matching networks [5–7], switchable matching networks [8, 9], and aperture tuning [10], but all these methods do not provide solutions to tune multiple frequency bands independently. In [11], we presented the initial measurements, and this article extends the analysis by showing a significantly broader set of experimental results that are further used to optimize the transponder operation at different frequencies. The optimization of the delays of the modulating signals is implemented with an automatized system for a measured prototype transponder, while it was only simulated in [11]. The theoretical basis of the work is also developed further, for instance, by taking into account the duty cycle of the modulating signal.

Manuscript received 1 September 2020.

T. A. Siddiqui, J. Holopainen, and V. Viikari are with the Department of Electronics and Nanoengineering, Aalto University, School of Electrical Engineering, Espoo 02150, Finland; e-mail: tauseef.siddiqui@aalto.fi, jari.holopainen@aalto.fi, ville.viikari@aalto.fi.

P. Khanal is with the Department of Electrical Engineering, Chalmers University of Technology, Hörsalsvägen 11, Göteborg, 41296, Sweden; e-mail: prabhat@chalmers.se.

The work of T. A. Siddiqui is supported, in part, by the Aalto Doctoral School of Electrical Engineering, Finland and in part by the University College of Engineering and Technology, The Islamia University of Bahawalpur, Pakistan.

2. Theory

Figure 1 exhibits the working principle of the broadband transponder. It is designed by using multiple modulators and a cluster of monopole antennas to achieve a continuously reconfigurable operation. In the antenna cluster, the elements differ in shape, size, and spacing, and each antenna element has a different resonating frequency. If the antenna cluster is matched, the modulated signal $f_{\mathrm{RF}} \pm f_{\mathrm{mod}}$ (signal b_1 accepted by the reader antenna at port 1) will reflect and deliver the intended data back to the reader. This is the signal of interest to be maximized in this work. When the load ($\rho_{\mathrm{load2,..,}N}$) at each port is switched between a short and open circuit, it creates a time domain reflection coefficient that varies from $\rho_s = -1$ to $\rho_o = +1$. The switching of load impedances creates a modulation, and the mixed modulated signal ($a_{2,..,N}$) reflects back at the input of the switch. The modulated backscattered signal ($b_{2,..,N}$) is proportional to the difference of the reflection coefficients $\left|\rho_{\mathrm{short}} - \rho_{\mathrm{open}}\right|$ of the two load impedances. This is derived from the complex Fourier series by integrating the time domain reflection coefficient of the load over one period (i.e., from 0 to $T = 1/f_{\mathrm{mod}}$). This is calculated as

$$\rho_{\mathrm{load}n} = \frac{j}{\pi}(\rho_s - \rho_o)e^{-jd_n\omega_{\mathrm{mod}}}(1 - e^{-j2\pi Dc}) \qquad (1)$$

in which $\omega_{\mathrm{mod}} = 2\pi f_{\mathrm{mod}}$, where $f_{\mathrm{mod}} = 1/T$ is the modulation frequency, d_n is the time delay of the square signal used for modulation, and Dc represents the effect

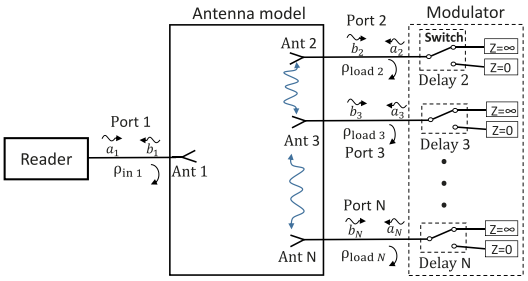

Figure 1. Broadband transponder working principle with switchable loads.

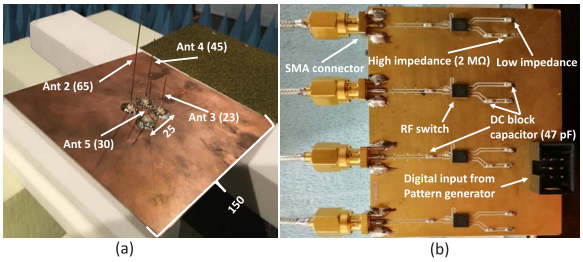

Figure 2. Transponder prototype with all dimensions in millimeters. (a) Manufactured antenna cluster. (b) Modulators PCB circuit.

of the duty cycle. In this work, the performance of the transponder is investigated at the first harmonic only hence, and (1) fulfills modeling the transponder. The duty cycle of 50% maximizes the scattered power compared with other values of the duty cycle. Hence, we use this value in our work.

Consider an N-port network as shown in Figure 1; the input reflection coefficient at port 1 is $\rho_{\text{in1}} = b_1/a_1$, and the load reflection coefficients at ports 2,3, N are $\rho_{\text{load}n} = a_n/b_n$. The system scattering matrix can be rewritten as

$$\begin{bmatrix} b_1 \\ b_2 \\ \vdots \\ b_N \end{bmatrix} = \begin{bmatrix} S_{11} & S_{12} & \dots & S_{1N} \\ S_{21} & S_{22} & \dots & S_{2N} \\ \vdots & \vdots & \ddots & \vdots \\ S_{N1} & S_{N2} & \dots & S_{NN} \end{bmatrix} \begin{bmatrix} b_1/\rho_{\text{in1}} \\ b_2\rho_{\text{load2}} \\ \vdots \\ b_N\rho_{\text{loadN}} \end{bmatrix} \quad (2)$$

The reflection coefficient of the reader antenna ($S_{11} = 0$) does not affect the reflected modulated signal $b_{1,\text{mod}}$ and must be subtracted. By solving (2), the modulated reflection coefficient ($\delta\rho_{\text{in1}}$) at port 1, when the transponders have four coupled antenna elements, i.e., $N = 5$ can be written [12] as

$$\delta\rho_{\text{in1}} = \frac{-S_{21}D_2 + S_{31}D_3 - . + S_{51}D_5}{D_1} \quad (3)$$

where D_N are the determinants of the minors, obtained of the matrix $(\mathbf{A\text{-}I})^H$. The delay values of (3) are optimized to give the largest modulated reflection coefficient $\delta\rho_{\text{in1}}$. To validate our theory, the transponder model is designed, and measurement results are presented.

3. Transponder Prototype

Figure 2 depicts the dimensions of manufactured antenna cluster along with the modulator PCB circuit used in this work. The antenna cluster is modeled in CST Microwave Studio Suite, version 2020, and printed circuit board (PCB) is designed by using PADS circuit designer, version VX.2.2, 2017. The antenna cluster is grouped together in a 2 × 2 configuration with the diagonal spacing of 25 mm on the squared ground plane. The resonant frequencies of the four monopoles are chosen so that they extend over and cover the whole band of interest (1 GHz to 6 GHz). A monopole has multiple resonances, and with this sort of spacing of resonant frequencies, the transponder can operate across a wide frequency band. Figures 3 and 4 show the reflection and coupling coefficients of antenna elements, respectively. The design is done so that at least some of the elements are simultaneously matched and mutually coupled at a given frequency for the purpose of achieving the constructive interference. This allows maximizing the total reflected modulated signal on the basis of the constructive interference of the optimally phased reflected modulated signals of the mutually coupled monopoles. For the minimum total reflected signal, the destructive interference happens with the nonoptimal phasing of the modulated reflected signals. Unlike antenna arrays, this technique in the antenna cluster benefits from the mutual coupling instead of avoiding it.

Explicit design rules for cluster antennas have only been derived for a two-antenna case [12]. The analysis in the article shows that the coupling and port reflections need to be correctly related to achieve good active matching. However, no similar analytical equations have been derived for antennas with a larger number of ports. As the number of ports increase, the system becomes more complex. Note that even for two antennas, there is an infinite number of solutions resulting in perfect active matching. If the matching is extremely poor (e.g., –3 dB), weighting of the signals will not help in canceling the reflections, the optimal

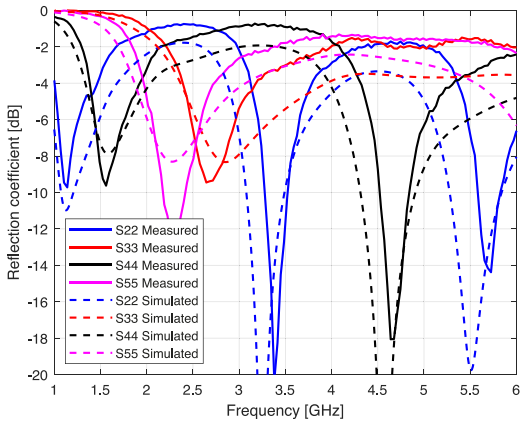

Figure 3. Reflection coefficients as a function of frequency.

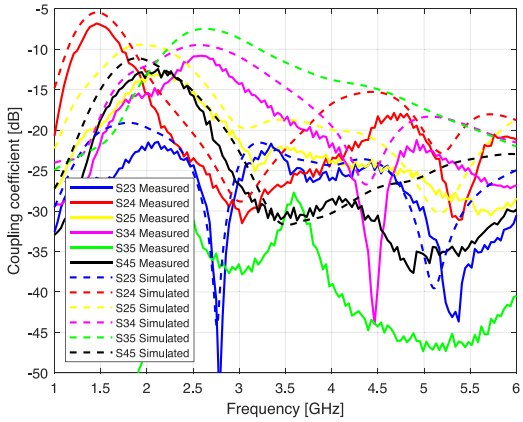

Figure 4. Coupling coefficients as a function of frequency.

range of the matching should be around −5 dB to −7 dB to have the benefit of coupling in a coupled antenna cluster environment [4, 12–17]. Matching depends on s parameters, and it is not easy to drive definitive criteria. The outputs of the RF switches are connected to 2 MΩ resistors for high-impedance termination (open circuit) and to the ground directly for low-impedance termination (short circuit). The input and output of the switches are connected to dc block capacitors of 47 pF. The SPDT RF switches (VSWA2-63DR+) are from mini-circuits and lumped components are from Murata. For ideal short and open circuit terminations, difference in the reflection coefficient $|\delta\rho| = |\rho_1 - \rho_2| = 2$, but in real practice, $|\delta\rho\ |$ is less than 2. The load impedances of the modulator PCB circuit are measured with the vector network analyzer at different ports. Note that the modulator circuit is working sufficiently well across the desired frequency range, and $(|\rho_1 - \rho_2|)$ is well between 1 and 1.6, except at few frequencies.

4. Automation of Measurement Setup

The measurements are performed in the anechoic chamber of Aalto University, School of Electrical Engineering, Espoo, Finland. It consists of a signal generator (R&S SMP 22), signal analyzer (R&S FSIQ 40), pattern generator (Agilent 16720A-1), and transmitting (Tx) and receiving (Rx) antennas (ETS Lindgren 3164-08 quad-ridged horn antennas). The reader antenna (Tx) transmits the power of +27 dBm from the signal generator at a single frequency that shifts from 1 GHz to 6 GHz. The broadband transponder picks up this signal and backscatters a modulated signal that is received by the other reader antenna (Rx) and is measured with the signal analyzer. Modulation frequency f_{mod} is set to 1 MHz (i.e., signal of the 1000 ns time period with a 50% duty cycle) from the pattern generator for four modulators. For the selection of f_{mod}, it should be large enough so that we can separate the useful information from the unmodulated wave. On the other hand, the modulation frequency should be small enough so that the modulated signal does not fall outside the system band. Additionally, the high

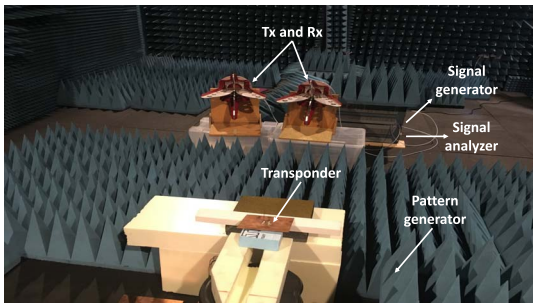

Figure 5. Measurement setup used in the anechoic chamber for this work. The distance (1.6 m) from the transponder to the Tx and Rx antennas is the same to ensure the far-field conditions. The Tx and Rx antennas are set to vertical polarization.

modulation frequency also leads to increased modulation power consumption. As a trade-off between these factors, we have chosen the 1 MHz modulation frequency. The delay resolution of 100 ns is chosen for the time period signal of 1000 ns for each modulator, which can be transmitted with 10 possible different digital logic pulses by using a pattern generator. There are four digital control signals in one single delay set for four modulators, and one of the digital control signals is kept constant as a reference. With this configuration, there can be 1000 combinations of delay sets ($10^3 = 1000$). The four channels of pattern generators are used to generate the user-defined patterns (delay sets) of digital logic high–low pulses. In this article, we demonstrate measurement results with all the possible 1000 delay set combinations. The measurement setup shown in Figure 5 is automated to run these combinations of delay sets to find the optimal delay distribution at which the transponder would backscatter the maximum received power at a given frequency. The automation is done by controlling the signal analyzer and the signal generator via the general purpose interface bus, and the pattern generator is controlled through the local area network interface with a personal computer running LabVIEW, version 2019, virtual instrumentation.

5. Measurement Results and Discussion

Figure 6 depicts the effect of delaying on backscattered received power as a function of delay set distribution generated by the pattern generator systematically. In Figure 6, the results are sorted out with increasing the received power. The results illustrate that the first 200 delay combination sets are more productive in improving the received power across all frequency ranges. The curves remain somewhat flat after the 200 delay set distribution, and there is gradual change in the received power. The resolution of the delaying does not need to be as accurate as 100 ns in practice, because there is no significant improvement in the backscattered signal after 200 delay sets. So, more coarse resolution would be enough, at least with this system. This might be

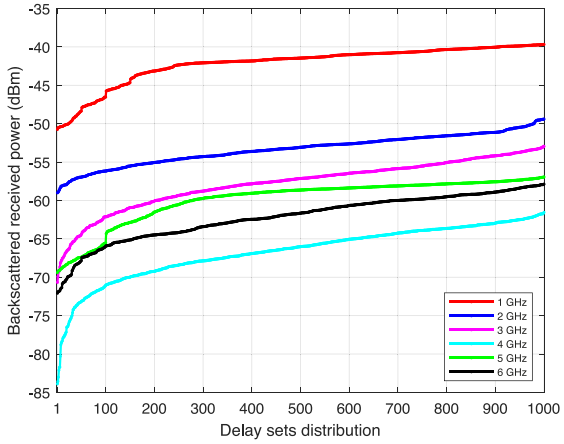

Figure 6. The effect of delaying on received power as a function of delay set distribution.

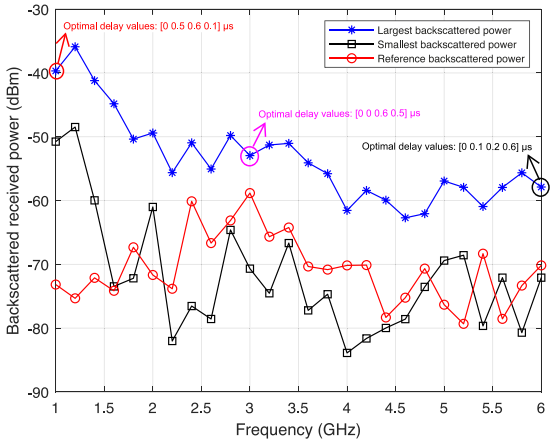

Figure 7. Received power comparison of the studied broadband transponder.

meaningful information when considering the practical implementation on the basis of a very low-powered microcontroller.

Figure 7 shows the comparison between the maximum and minimum backscattered received power obtained through delaying as a function of frequency of the studied broadband transponder. The difference between maximum and minimum received powers, which is caused by the delaying, is at least 10 dB and even up to 28 dB, depending on the frequency. It shows that the delaying has a very significant effect on the received power, and when the optimal phasing is chosen, the transponder backscatters the maximum received power. The comparison is also shown with the reference transponder. The reference transponder consists of a single monopole antenna that is tuned at a resonant frequency of 3 GHz. Hence, the reference is similar with that of the 23 mm monopole of the antenna cluster whose resonance frequency is 2.7 GHz (see Figure 3). In comparison with reference transponder, the enhancement in the backscattered received power is up to 39 dB, and even a 6 dB improvement is achieved at a frequency of 3 GHz, where the reference transponder is tuned.

On the basis of the aforementioned results, the broadband transponder seems to perform better at lower frequencies, and there is a decreasing trend in the received power levels at the higher frequencies. The reason is that modulator (i.e., $|\rho_1 - \rho_2|$) is stronger at lower frequencies than at higher frequencies. The other explanation for this behavior is that the physically largest monopoles have bigger effective aperture areas than the shorter monopoles. Hence, the power received and backscattered by large monopoles is higher than the power backscattered by shorter monopoles. Also, the radiation pattern at the fundamental resonance ($\lambda/4$) of monopoles radiates more toward the reader antenna as compared with the multiple resonance modes that are at higher frequencies [18]. Although the received power levels differ, depending on the frequency, the backscattered power is maximized with the optimal phasing as compared with nonoptimal phasing. Figure 7 also shows the importance of correct phasing (blue curve) because with the nonoptimal phasing (black curve), the broadband transponder performs poorly at certain frequencies as compared with the reference transponder. The results in this work are already encouraging, but by further optimizing the antenna structure, it is possible to make the functioning of the broadband transponder even more efficient, and the stronger backscattered signal power over the desired frequency range can be acquired.

6. Conclusion

On the basis of the findings of this article, the transponder performance can be taken into consideration for future low-energy smart devices. Future work includes the practical implementation of optimal phasing by using the digital integrated circuit chip for the optimization of backscattered received power. Design principles for an antenna cluster should also be investigated to work effectively at any frequency.

7. References

1. N. Van Huynh, D. T. Hoang, X. Lu, D. Niyato, P. Wang, et al., "Ambient Backscatter Communications: A Contemporary Survey," *IEEE Communications Surveys & Tutorials*, **20**, 4, May 2018, pp. 2889-2922.
2. C. Yang, J. Gummeson, and A. Sample, "Riding the Airways: Ultra-Wideband Ambient Backscatter via Commercial Broadcast Systems," IEEE Infocom 2017–IEEE Conference on Computer Communications, Atlanta, GA, USA, May 1–4, 2017, pp. 1-9.
3. S. N. Daskalakis, J. Kimionis, A. Collado, G. Goussetis, M. M. Tentzeris, et al., "Ambient Backscatterers Using FM Broadcasting for Low Cost and Low Power Wireless Applications," *IEEE Transactions on Microwave Theory and Techniques*, **65**, 12, December 2017 pp. 5251-5262.
4. J.-M. Hannula, J. Holopainen, and V. Viikari, "Concept for Frequency Reconfigurable Antenna Based on Distributed Transceivers," *IEEE Antennas and Wireless Propagation Letters*, **16**, August 2017, pp. 764-767 doi: 10.1109/LAWP.2016.2602006.

5. J. Ilvonen, R. Valkonen, J. Holopainen, and V. Viikari, "Multiband Frequency Reconfigurable 4G Handset Antenna with MIMO Capability," *Progress in Electromagnetics Research,* **148**, August 2014, pp. 233-243, doi: 10.2528/PIER14062703.
6. S. Caporal Del Barrio, A. Tatomirescu, G. Pedersen, and A. Morris, "Novel Architecture for LTE World-Phones," *IEEE Antennas and Wireless Propagation Letters,* **12**, INSPEC Accession Number: 14066587, Volume 12, December, 2013, pp. 1676-1679, doi: 10.1109/LAWP.2014.2301014.
7. R. Valkonen, C. Luxey, J. Holopainen, C. Icheln, and P. Vainikainen, "Frequency-Reconfigurable Mobile Terminal Antenna With MEMS Switches," 4th European Conference on Antennas and Propagation, Barcelona, Spain, April 12–16, 2010, pp. 1-5.
8. R. Valkonen, J. Holopainen, C. Icheln, and P. Vainikainen, "Broadband Tuning of Mobile Terminal Antennas," Second European Conference on Antennas and Propagation, Edinburgh, UK, November 11–16, 2007, pp. 1-6.
9. R. Valkonen, M. Kaltiokallio, and C. Icheln, "Capacitive Coupling Element Antennas for Multi-Standard Mobile Handsets," *IEEE Transactions on Antennas and Propagation*, **61**, 5, May 2013, pp. 2783-2791.
10. D. Rodrigo, B. A. Cetiner, and L. Jofre, "Frequency, Radiation Pattern and Polarization Reconfigurable Antenna Using a Parasitic Pixel Layer," *IEEE Transactions on Antennas and Propagation*, **62**, 6, June 2014, pp. 3422-3427.
11. T. A. Siddiqui, P. Khanal, J. Holopainen, and V. Viikari, "Broadband Transponder Based on Frequency-Reconfigurable Cluster Antenna and Phased Modulators," *IEEE Antennas and Wireless Propagation Letters*, **19**, 2, February 2020, pp. 238-242.
12. J.-M. Hannula, A. Lehtovuori, R. Luomaniemi, T. O. Saarinen, and V. Viikari, "Beneficial Interaction of Coupling and Mismatch in a Two-Antenna System," 2019 13th European Conference on Antennas and Propagation, Krakow, Poland, March 31–April 5, 2019, pp. X-X.
13. J. X. Yun and R. G. Vaughan, "A View of the Input Reflection Coefficient of the N-Port Network Model for MIMO Antennas," 2011 IEEE International Symposium on Antennas and Propagation, Spokane, WA, USA, July 3–8, 2011, pp. 297-300.
14. J.-M. Hannula, J. Holopainen, and V. Viikari, "Further Investigations on the Behavior of a Frequency Reconfigurable Antenna Cluster," 2017 11th European Conference on Antennas and Propagation, Paris, France, March 19–24, 2017, pp. X-X.
15. J.-M. Hannula, T. Saarinen, J. Holopainen, and V. Viikari, "Frequency Reconfigurable Multiband Handset Antenna Based on a Multichannel Transceiver," *IEEE Transactions on Antennas and Propagation*, **65**, 9, September 2017, pp. 4452-4460.
16. J.-M. Hannula, T. O. Saarinen, A. Lehtovuori, J. Holopainen, and V. Viikari, "Tunable Eight-Element MIMO Antenna Based on the Antenna Cluster Concept," *IET Microwave Antennas and Propagation*, **13**, 7, February 2019, p. 959, doi: 10.1049/ietmap.2018.5742.
17. J.-M. Hannula, M. Kosunen, A. Lehtovuori, K. Rasilainen, K. Stadius, et al., "Performance Analysis of Frequency-Reconfigurable Antenna Cluster with Integrated Radio Transceivers," *IEEE Antennas and Wireless Propagation Letters*, **17**, 5, May 2018, pp. 756-759.
18. W. L. Stutzman and G. A. Thiele, *Antenna Theory and Design*, 3rd Ed., Hoboken, NJ, Wiley, 2012.